2005 American Control Conference
June 8-10, 2005. Portland, OR, USA

Optimization-Based Correction of a Segmented Optical Telescope Using Image-Plane Sensing

Philip D. Olivier and Dennis S. Bernstein

Abstract— **The apertures of many optical telescopes are constructed of multiple mirror segments. To attain the performance of a monolithic mirror, the segments must be corrected in tip, tilt, and piston. In this paper we consider a three-segment optical telescope and develop an optimization-based algorithm for determining the initial error of the segmented aperture through a sequence of displacements, thereby facilitating correction of the initial error. The optimization algorithm is used to investigate the effects of sensor quantization on the achievable correction accuracy.**

I. Introduction

Because of difficulties in fabricating, transporting, and maintaining the shape of large apertures, optical telescopes are often constructed of multiple mirror segments. However, even if rigid, the segments of the mirror array must be corrected in tip, tilt, and piston to meet a variety of specifications [1, pp. 332–337], [2]. Tip and tilt adjustment involves rotating the mirror segments to coalign the images from all of the mirror segments on the focal plane. Piston adjustment involves translating the mirror segments to equalize the optical path distances and thus ensure that the images are of the same size. Finally, cophasing is needed to eliminate discontinuities between possibly nonrigid segments having different focal lengths. A typical cophasing specification is $\lambda/28$, which corresponds to about 60 nanometers at $\lambda = 1.5$ microns.

The literature on mirror segment correction is extensive. Standard techniques are based on interferometry and related instrumentation [1, pp. 332–337]. Alternatively, image-plane sensing provides an economical alternative, especially for space-based applications [3, 4]. Hence there is interest in developing algorithms for moving the mirror segments and processing the data for efficiently determining the required adjustments. In [5], a multi-observer algorithm is used to asymptotically determine the segment errors after a sequence of adjustments.

In the present paper we consider a three-segment optical telescope motivated by the Deployable Optical Telescope (DOT) project [6], and develop an optimization-based algorithm for determining and correcting the segment errors. First, we consider the case of piston alignment only, and then we consider tip, tilt, and piston correction. The optimization algorithm is used to investigate the effect of sensor quantization on the achievable alignment accuracy.

This work was supported by the Air Force Research Laboratory, Albuquerque, NM

Philip D. Olivier is with the Electrical and Computer Engineering Department, Mercer University, Macon, Georgia 31207 Olivier_PD@mercer.edu

Dennis S. Bernstein is with the Department of Aerospace Engineering, University of Michigan, Ann Arbor, MI dsbaero@umich.edu

II. Piston Correction

Piston correction for a three-segment telescope requires two piston adjustments. The kinematic model is given by

$$x_{k+1} = x_k + u_k, \tag{1}$$

where $k = 0, 1, \ldots$, the input u_k denotes the adjustment of the piston at step k, and the components of $x_k \triangleq \left[\begin{array}{c} x_{1k} \\ x_{2k} \end{array}\right]$ are the piston displacements of two of the segments relative to the third segment. Under monochromatic illumination with wavelength λ, the intensity measurement at the center of the coaligned beam is given by

$$\begin{aligned} y_k &= 3 + 2\cos[(4\pi/\lambda)x_{1k}] + 2\cos[(4\pi/\lambda)x_{2k}] \\ &+ 2\cos[(4\pi/\lambda)(x_{1k} - x_{2k})]. \end{aligned} \tag{2}$$

Since reflected light must travel twice the length of a mirror displacement, the measurement y_k is unchanged if x_{1k} or x_{2k} is perturbed by an integer multiple of $\lambda/2$. Therefore, without loss of generality, we assume that the piston displacements are confined to the closed-open interval $[0, \lambda/2)$. In Section 4 the measurement function h will be obtained as a special case of the expression for illumination intensity, where additional physical constants appear.

Consider the measurement function $h : [0, \lambda/2) \times [0, \lambda/2) \to \mathbb{R}$ defined by

$$\begin{aligned} h(x_1, x_2) &\triangleq 3 + 2\cos[(4\pi/\lambda)x_1] + 2\cos[(4\pi/\lambda)x_2] \\ &+ 2\cos[(4\pi/\lambda)(x_1 - x_2)] \end{aligned} \tag{3}$$

whose gradient is given by

$$h'(x_1, x_2) = \frac{8\pi}{\lambda} \left[\begin{array}{c} -\sin((4\pi/\lambda)x_1) - \sin[(4\pi/\lambda)(x_1 - x_2)] \\ -\sin[(4\pi/\lambda)x_2] + \sin[(4\pi/\lambda)(x_1 - x_2)] \end{array}\right]^{\mathrm{T}}, \tag{4}$$

where "T" denotes transpose. The gradient $h'(x_1, x_2)$ vanishes if and only if (x_1, x_2) is one of the points $(0, 0)$, $(0, \lambda/4)$, $(\lambda/4, 0)$, $(\lambda/6, \lambda/3)$, $(\lambda/3, \lambda/6)$. In fact, $h(0, 0) = 9$ is the maximum value of h, and $h(\lambda/6, \lambda/3) = h(\lambda/3, \lambda/6) = 0$ is the minimum value of h. Thus, h is onto $[0, 9]$, but is not one-to-one. In fact, for all $x_1, x_2 \in [0, \lambda/2)$,

it follows that $h(\lambda/2, x_2) = h(x_1, \lambda/2) = 1$, while, if $x_2 = x_1 \pm \lambda/4$, then $h(x_1, x_2) = 1$. Figure 1 shows a contour plot of h.

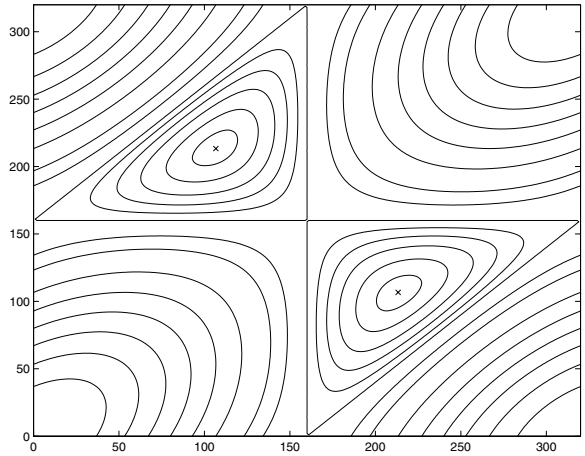

Fig. 1. Contour plot of the measurement function h for $\lambda = 640$ nm. The measurement function $h(x_1, x_2)$ attains its (global) minimum value of 0 at $(\lambda/6, \lambda/3)$ and $(\lambda/3, \lambda/6)$ (denoted by '$\times$'), and its (global) maximum value of 9 at $(0, 0)$, $(0, \lambda/2)$, $(\lambda/2, 0)$, and $(\lambda/2, \lambda/2)$. Along the horizontal, vertical, and diagonal lines, h attains the value of 1.

Our goal is to determine the initial displacement x_0. To do this, we consider a sequence of r displacement inputs $u_0, \ldots, u_{r-1}$ and define the cumulative displacement inputs $U_0, \ldots, U_{r-1}$ by

$$U_k \triangleq \sum_{i=0}^{k} u_i. \tag{5}$$

Consequently, for $k = 0, 1, \ldots, r-1$,

$$x_{k+1} \triangleq x_0 + U_k. \tag{6}$$

Of course,

$$u_k = U_k - U_{k-1}. \tag{7}$$

Once x_0 is determined by the method developed below, the final correction step is achieved by choosing $U_r = -x_0$, that is, $u_r = U_r - U_{r-1} = -x_0 - U_{r-1}$, so that $x_{r+1} = 0$. Hence, with r input displacements and corresponding measurements, the desired correction is achieved a single additional displacement.

Next, we consider r measurements $y_1, \ldots, y_r$ given by (2) and define the *fit error* $J : [0, \lambda/2) \times [0, \lambda/2) \to [0, \infty)$ by

$$J(x) \triangleq \sum_{i=0}^{r-1} [h(x + U_i) - y_{i+1}]^2. \tag{8}$$

We then seek $x \in [0, \lambda) \times [0, \lambda)$ that minimizes J. Note that $h(x_0 + U_i) = h(x_{i+1}) = y_{i+1}$, and thus $J(x_0) = 0$ so that x_0 is a global minimizer of J (note that J assumes nonnegative values, and thus any zero of J is necessarily a global minimizer). Since h is not one-to-one, J does not necessarily have a unique global minimizer. Furthermore, the local minimizers of J depend on the choice of $U_0, \ldots, U_{r-1}$. (A global minimizer is a local minimizer that yields the lowest possible value of $J(x_0)$.

In practice, exact measurements of $h(x + U_i)$ are not available, and thus y_i is generally corrupted by noise. For example, if y_i is measured by means of an 8-bit A-to-D converter over ± 1 V, then each measurement y_i is corrupted by a uniformly distributed random variable in the interval $[-0.0176, 0.0176]$, where $0.0176 \approx (1/2)9/2^8$. Letting $\hat{y}_i$ denote a noisy measurement of y_i so that $\hat{y}_i$ differs from y_i due to the addition of a random perturbation due to noise, the *perturbed fit error* $\hat{J} : [0, \lambda/2) \times [0, \lambda/2) \to [0, \infty)$ is defined by

$$\hat{J}(x) \triangleq \sum_{k=0}^{r-1} [h(x + U_k) - \hat{y}_{k+1}]^2. \tag{9}$$

Because of measurement noise, it is not generally true that $\hat{J}(x_0) = 0$, and x_0 need not be a global minimizer of $\hat{J}$. In fact, a global minimizer $\hat{x}_0$ of $\hat{J}$ may or may not be close to a global minimizer x_0 of J, although it is reasonable to assume that, if the measurement noise is small, then a global minimizer of $\hat{J} = 0$ will be close to x_0. In the next section we use numerical optimization to minimize $\hat{J}$ and assess the effect of sensor quantization on our ability to determine x_0.

III. Optimization-Based Piston Correction

In this section we use gradient-based optimization to determine local minimizers of $\hat{J}$, and then choose the local minimizer $\hat{x}_0$ with the lowest cost to provide an estimate of x_0. Since the measurement function h has multiple local minimizers, $\hat{J}$ generally has multiple local minimizers as well. Although the local minimizers of $\hat{J}$ are determined by the choice of displacement inputs $u_0, \ldots, u_{r-1}$, it is not apparent how to choose $u_0, \ldots, u_{r-1}$ to reduce the number of local (or global) minimizers of $\hat{J}$ or to facilitate the computation of a global minimizer. Finally, as already mentioned, the measurement noise corrupting $y_1, \ldots, y_r$ perturbs the locations of the local minimizers of J, which impedes the ability to determine the desired global minimizer x_0 of J. Nevertheless, our goal is to determine, as best we can, a global minimizer of $\hat{J}$, and assess how well this global minimizer approximates the initial displacement x_0, which is a global minimizer of J.

On the other hand, cases in which J or $\hat{J}$ have multiple global minimizers are nongeneric, and numerical experiments suggest that an increase in the number r of displacement inputs decreases the likelihood that J or $\hat{J}$ has multiple global minimizers. Assuming that a global minimizer of $\hat{J}$ can be found, it remains to be determined how the location of the global minimizer is perturbed by the presence of sensor quantization noise. In essence, we are interested in knowing to what extent a perturbation of a

nonconvex cost function perturbs the location of the global minimizer. We have not found this problem addressed in the optimization literature.

Although global optimization methods can be used to determine a global minimizer of $\hat{J}$, we use a locally convergent gradient-based method applied multiple times with different starting estimates of x_0 to improve the ability to determine a global minimizer. For optimization, we use the Matlab routine *fminunc*, which is a quasi-Newton gradient-based algorithm. We run fminunc multiple times and choose the local minimizer with the lowest value of $\hat{J}$. The starting estimate for x_0 is randomly generated, and the cumulative displacement inputs $U_0, \ldots, U_{r-1}$ are randomly generated to have uniformly distributed components over $[-\lambda/4, \lambda/4]$. We then run fminunc for a maximum number of iterations and choose the computed local minimizer $\hat{x}_0$ yielding the smallest value of $\hat{J}(\hat{x}_0)$.

To demonstrate this procedure, we apply fminunc for $r = 3, 5$ input displacements with sensor quantization resolution ranging from 0.001 to 0.015 in increments of 0.001. For each value of r and for each noise level, we apply the optimization algorithm to 25 randomly generated choices of $U_0, \ldots, U_{r-1}$ and x_0. To determine a global minimizer for each problem, fminunc is run 15 times with randomly generated initial estimates of x_0. For the 25 choices, we compute the median (over random choices) average (over segments) error in determining the initial piston displacements normalized by half the wavelength. The numerical results, shown in Figure 2, indicate that the ability to determine the initial displacement increases with an increasing number of input displacements and decreases with larger (that is, poorer) sensor resolution.

For all computations, the wavelength λ and the piston displacements are expressed in nanometers. It was found that representing $\lambda = 640$ nm in meters results in poor numerical conditioning.

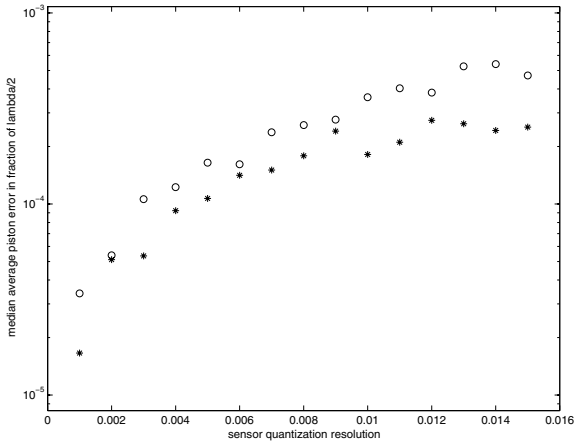

Fig. 2. Median of the average piston error normalized by half the wavelength. Both 3 and 5 measurements are considered under different levels of sensor quantization resolution. The median is determined over 25 randomly generated choices of piston input displacements and piston errors for each resolution level and number of measurements. Legend: '$\circ$' is 3 measurements, '$*$' is 5 measurements. A locally convergent gradient-based algorithm is run 15 times with a randomly generated starting point to help determine a global minimizer.

IV. Tip, Tilt, and Piston Correction

In this section we continue to assume that the optical telescope has three mirror segments with monochromatic illumination at wavelength λ. As shown in [3, 4], the electric field strength in V/m at a point $\vec{u} = \begin{bmatrix} \hat{u} \\ \hat{v} \end{bmatrix}$ in the image plane of a segmented mirror is given by

$$E(\vec{u}) = \sqrt{\frac{2}{c\varepsilon_0}} \sum_{i=1}^{3} \frac{A_i \sqrt{I_i}}{\lambda z} S_i(\|r_i\|) e^{\jmath \frac{4\pi}{\lambda} p_i} e^{\jmath \frac{2\pi}{\lambda z} \vec{u} \cdot \vec{\xi}_i}, \quad (10)$$

where $\jmath \triangleq \sqrt{-1}$, c is the speed of light in m/s, ε_0 is the permittivity of the medium, which, for free space, is 8.8542×10^{-12} C^2/N-m^2, z is the focal length of the array, and, for $i = 1, 2, 3$, A_i is the area of the ith segment, I_i is the intensity of light illuminating the ith segment in units watt/m^2, p_i is the piston displacement of the ith segment, $\vec{\xi}_i$ is the location of the center of the ith segment relative to the origin of an aperture coordinate frame thus reflecting the geometric arrangement of the mirror array (for example, linear or circular), and $S_i(\cdot)$ is the *segment function* of the ith segment, as described below. If the actual distance varies among segments by an integral number of wavelengths, then the combined image will not be coaligned. However, in practice, the actual optical path distance can vary among segments by a small integral number of wavelengths without substantial image degradation through image size variation. The light intensity $I(\hat{u}, \hat{v})$ at $\vec{u}$ in watt/m^2 is thus given by [7, p. 49]

$$I(\hat{u}, \hat{v}) = \frac{1}{2} c\varepsilon_0 |E(\vec{u})|^2. \quad (11)$$

The dimensionless segment function S_i is determined by the shape of the ith mirror segment. We assume circular mirror segments, in which case [4]

$$S_i(\|r_i\|) = 2 \frac{J_1(\frac{\pi d_i \|r_i\|}{\lambda z})}{\frac{\pi d_i \|r_i\|}{\lambda z}}, \quad (12)$$

where

$$r_i \triangleq \vec{u} + \frac{\lambda z}{2\pi} \nabla^{\mathrm{T}} \varphi_i = \begin{bmatrix} \hat{u} + 2z t_{\hat{v}i} \\ \hat{v} + 2z t_{\hat{u}i} \end{bmatrix}, \quad (13)$$

$\|\cdot\|$ denotes the Euclidean norm, J_1 is the Bessel function of the first kind of order 1, d_i is the diameter of the ith segment, $A_i \triangleq \pi(d_i/2)^2$, and the tip and tilt rotation angles of the ith segment are given by

$$\begin{bmatrix} t_{\hat{v}i} \\ t_{\hat{u}i} \end{bmatrix} \triangleq \frac{\lambda}{4\pi} \nabla^{\mathrm{T}} \varphi_i, \quad (14)$$

and $\varphi_i = \varphi_i(\vec{u})$ denotes the phase distribution ahead of a reference (idealized) surface within the ith segment. Note that $t_{\hat{v}i}$ is the rotation of the mirror segment about the $\hat{u}$ axis, while $t_{\hat{u}i}$ is the rotation of the mirror segment about the $\hat{v}$ axis.

Since [8, p. 99, (5.2.3)]

$$J_1(r) = \frac{r}{2} - \frac{r^3}{16} + - \cdots \tag{15}$$

it follows that

$$\lim_{r \to 0} J_1(r)/r = 1/2. \tag{16}$$

Hence, $S_i(0) = 1$.

Next, we assume without loss of generality that $p_3 = 0$. Consequently, the kinematics are modeled by (1), where x_k is the vector with 8 components defined by (suppressing the subscript k)

$$x \stackrel{\triangle}{=} \left[\begin{array}{cccccccc} p_1 & p_2 & t_{\hat{v}1} & t_{\hat{u}1} & t_{\hat{v}2} & t_{\hat{u}2} & t_{\hat{v}3} & t_{\hat{u}3} \end{array} \right]^{\mathrm{T}}, \tag{17}$$

where p_1, p_2 denote the piston displacements of the first two segments.

As a special case of (10), assume $\varphi_1 = 0$ so that there is no initial tip or tilt, consider identical apertures with area A and identical illumination I, and set $\vec{u} = 0$. Then, it follows from (10) that

$$\begin{aligned} I(0,0) &= \left(\frac{A\sqrt{I}}{\lambda z} \right)^2 \left| \sum_{i=1}^{3} S_i(0) e^{\jmath \frac{4\pi}{\lambda} p_i} \right|^2 \\ &= \left(\frac{A\sqrt{I}}{\lambda z} \right)^2 \left| 1 + \sum_{i=1}^{2} e^{\jmath \frac{4\pi}{\lambda} p_i} \right|^2 \\ &= \left(\frac{A\sqrt{I}}{\lambda z} \right)^2 (3 + 2\cos[(4\pi/\lambda)p_1] \\ &\quad + 2\cos[(4\pi/\lambda)p_2] + 2\cos[(4\pi/\lambda)(p_1 - p_2)]) \\ &= \left(\frac{A\sqrt{I}}{\lambda z} \right)^2 h(p_1, p_2), \end{aligned} \tag{18}$$

where h is defined by (3).

Next, to correct the mirror array, let us define the measurement function $h : [0, \lambda/2)^2 \times [0, \pi/2)^6 \times \mathbb{R}^2 \to [0, \infty)$ by

$$h(x, \hat{u}, \hat{v}) \stackrel{\triangle}{=} I(\hat{u}, \hat{v}), \tag{19}$$

so that

$$h(x, \hat{u}, \hat{v}) = \left| \sum_{i=1}^{3} \frac{A_i \sqrt{I_i} \gamma_i}{\lambda z} S_i(\|r_i\|) e^{\jmath \beta p_i} \right|^2, \tag{20}$$

where

$$\beta \stackrel{\triangle}{=} \frac{4\pi}{\lambda}, \quad \gamma_i \stackrel{\triangle}{=} e^{\jmath \frac{2\pi}{\lambda z} \vec{u} \cdot \vec{\xi}_i}. \tag{21}$$

Next, note that

$$h(x, \hat{u}, \hat{v}) = h_0(x, \hat{u}, \hat{v}) \overline{h_0(x, \hat{u}, \hat{v})}, \tag{22}$$

where $\overline{(\cdot)}$ denotes complex conjugate and

$$h_0(x, \hat{u}, \hat{v}) \stackrel{\triangle}{=} \sum_{i=1}^{3} \frac{A_i \sqrt{I_i} \gamma_i}{\lambda z} S_i(\|r_i\|) e^{\jmath \beta p_i}. \tag{23}$$

Then, using the fact that

$$\frac{\partial |F(y)|^2}{\partial y} = 2\mathrm{Re} \left[\overline{F(y)} \frac{\partial F(y)}{\partial y} \right], \tag{24}$$

for $i = 1, 2$, it follows that

$$\frac{\partial h}{\partial p_i} = \frac{-2A_i \sqrt{I_i} \beta}{\lambda z} S_i(\|r_i\|) \mathrm{Im}\ \overline{h_0} \gamma_i e^{\jmath \beta p_i}. \tag{25}$$

Furthermore, we note that [8, p. 100, (5.2.6)]

$$J_1'(r) - \frac{1}{r} J_1(r) = -J_2(r), \tag{26}$$

where '$'$' denotes differentiation and J_2 is the Bessel function of the first kind of order 2. Hence,

$$\frac{\mathrm{d}}{\mathrm{d}r} \frac{J_1(r)}{r} = -\frac{J_2(r)}{r}. \tag{27}$$

Therefore, it follows that

$$\begin{aligned} \frac{\partial}{\partial t_{\hat{v}i}} S_i(\|r_i\|) &= \frac{-2\pi d_i}{\lambda z} \frac{J_2(\frac{\pi d_i \|r_i\|}{\lambda z})}{\frac{\pi d_i \|r_i\|}{\lambda z}} \frac{\partial \|r_i\|}{\partial t_{\hat{v}i}} \\ &= -\frac{4\pi d_i}{\lambda} (\hat{u} + 2z t_{\hat{v}i}) \hat{S}_i(\|r_i\|), \end{aligned} \tag{28}$$

where $\hat{S}_i(\cdot)$ is the function whose dimensions are $1/\text{length}$ given by

$$\hat{S}_i(\|r_i\|) \stackrel{\triangle}{=} \frac{J_2(\frac{\pi d_i \|r_i\|}{\lambda z})}{\frac{\pi d_i \|r_i\|^2}{\lambda z}}. \tag{29}$$

Consequently, for $i = 1, 2, 3$,

$$\frac{\partial h}{\partial t_{\hat{v}i}} = \frac{-8\pi d_i A_i \sqrt{I_i} (\hat{u} + 2z t_{\hat{v}i})}{\lambda^2 z} \hat{S}_i(\|r_i\|) \mathrm{Re}\ \overline{h_0} \gamma_i e^{\jmath \beta p_i}, \tag{30}$$

with a similar expression for $\partial h / \partial t_{\hat{u}i}$. To evaluate (30) we note that (15) and (26) imply that

$$\lim_{r \to 0} J_2(r)/r^2 = 1/8. \tag{31}$$

Hence, $\hat{S}_i(0) = \frac{\pi d_i}{8\lambda z}$.

V. Optimization-Based Tip, Tilt, and Piston Correction

As in Section 3, we consider a sequence of mirror-segment adjustments and use measurements of h given by (20) to estimate the initial tip, tilt, and piston given by x_0. To estimate x_0, we can consider either a single fixed choice of $(\hat{u}, \hat{v})$ or, using a camera image, we can obtain multiple values of h for each input displacement by considering different points $(\hat{u}, \hat{v})$ in the image plane corresponding to different camera pixels.

For tip, tilt, and piston correction, we define the fit error $J : [0, \lambda/2)^2 \times [0, \pi/2)^6 \times \mathbb{R}^2 \to [0, \infty)$ by

$$J(x) \triangleq \sum_{k=0}^{r-1} \sum_{j=1}^{n_k} [h(x + U_k, \hat{u}_{k,j}, \hat{v}_{k,j}) - y_{k+1,j}]^2, \quad (32)$$

where U_k is the cumulative input displacement given by (5), r is the number of input displacements, n_k is the number of image-plane measurements taken for each input displacement, $(\hat{u}_{k,j}, \hat{v}_{k,j})$ are the coordinates of the point in the image plane where the measurement is taken,

$$y_{k+1,j} = h(x_{k+1}, \hat{u}_{k,j}, \hat{v}_{k,j}) = h(x_0 + U_k, \hat{u}_{k,j}, \hat{v}_{k,j}), \quad (33)$$

and x_{k+1} is given by (1). As in the Section 3, we seek x that minimizes J. In the absence of measurement noise, $J(x_0) = 0$, and thus the initial displacement is a global minimizer of J (recall that J assumes nonnegative values, and thus every zero of J is a global minimizer). In the presence of measurement noise, a noisy measurement $\hat{y}_{k,j}$ of $y_{k,j}$ is available, and J is replaced by

$$\hat{J}(x) \triangleq \sum_{k=0}^{r-1} \sum_{j=1}^{n_k} [h(x + U_k, \hat{u}_{k,j}, \hat{v}_{k,j}) - \hat{y}_{k+1,j}]^2. \quad (34)$$

As in the case of piston correction only, the optimization algorithm fminunc is sensitive to the choice of units, and piston correction is most effective when λ and the piston displacements are expressed in nanometers. With $\nabla\varphi$ expressed in radians per meter, the tip and tilt angles are given in nanoradians. In this case, the fminunc algorithm performs best for corrections between -100 and +100 nanoradians, which suggests that tip and tilt angles in this range result in significant overlap of the images projected from the mirror segments as characterized by the segment functions. This range of angle corrections was thus used for Monte Carlo numerical experiments. For all of the numerical results presented below, we set $n_k = 1$ and consider only the point $(\hat{u}, \hat{v}) = (0, 0)$ in the image plane. System parameters were chosen to be $d_i = 1$ m for all segments, $z = 50$ m, and $\lambda = 640$ nm. For convenience we also set $I_i = (\lambda z / A_i)^2$ for all segments.

To demonstrate the procedure for tip, tilt, and piston correction, we apply fminunc for $r = 12$ input displacements with sensor quantization resolution ranging from 0.005 to 0.040 in increments of 0.005. The magnitudes of the measurements are such that the 0.005 quantization level corresponds to about a 0.2% noise-to-signal ratio. For each noise level, we apply the optimization algorithm to 6 randomly generated choices of $U_0, \ldots, U_{r-1}$ and x_0. To determine a global minimizer for each problem, fminunc is run 5 times with randomly generated initial estimates of x_0. For the 6 random choices of $U_0, \ldots, U_{r-1}$ and x_0, we compute the median (over random choices) average (over segments) error in determining the initial piston displacement normalized by half the wavelength as well as the median (over random choices) average (over segments) error in determining the initial tip and tilt displacement angles. The numerical results are shown in Figure 3 and Figure 4.

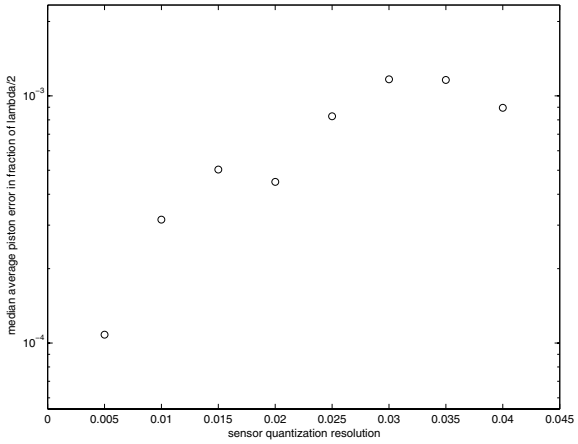

Fig. 3. Median of the average piston error normalized by half the wavelength. A total of 12 measurements are considered under different levels of sensor quantization resolution. The median is determined over 6 randomly generated choices of tip, tilt, and piston input displacements for each resolution level. The locally convergent gradient-based algorithm is run 5 times with a randomly generated starting point to help determine a global minimizer.

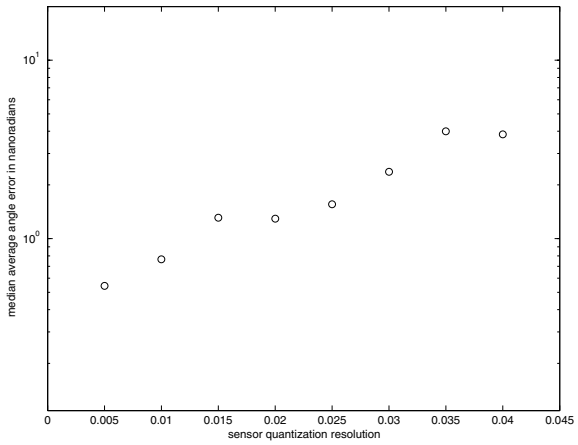

Fig. 4. Median of the average tip and tilt error normalized by half the wavelength. A total of 12 measurements are considered under different levels of sensor quantization resolution. The median is determined over 6 randomly generated choices of tip, tilt, and piston input displacements for each resolution level. The locally convergent gradient-based algorithm is run 5 times with a randomly generated starting point to help determine a global minimizer.

VI. Conclusions

In this paper we used a gradient-based nonlinear optimization algorithm with image-plane intensity measurements to correct the tip, tilt, and piston error in a 3-segment optical telescope. The effectiveness of the approach was quantified in the presence of noisy measurements.

There are several issues that warrant further investigation. First, the Matlab optimization algorithm fminunc was found to be sensitive to the units used to express piston displacements, although the source of this sensitivity is not apparent. It was also found that the algorithm worked well for a certain range of tip and tilt angles. It is of interest to relate this range to the overlap of the mirror segment images for specific mirror geometries. Next, since the optimization algorithm is capable of determining only local minimizers, the use of global optimization algorithms is of interest. Next, more extensive Monte Carlo simulation studies are needed to quantify the error in determining the necessary tip, tilt, and piston correction in the presence of sensor noise as a function of the number of mirror displacements. Finally, analogous questions for actuator noise are of interest.

From an optics point of view, there are several extensions of practical importance. First, application of the methodology to a segmented telescope with more than three segments will undoubtedly impact the numerical issues raised above. Next, the potential advantage of using polychromatic light remains to be investigated. A further extension involves the optimal use of multiple points in the image plane when a camera detector is used. The problem of tip/tilt coupling through image-plane misalignment is also of practical interest. Finally, while random generation of the mirror displacements U_k was found to be effective, it is of interest to develop optimal or suboptimal displacements yielding guaranteed correction accuracy. For example, initial displacements to bring the mirror images into approximate alignment provides a preliminary step for improving the effectiveness of the optimization-based solution.

VII. Acknowledgments

This research was supported in part by the Air Force Research Laboratory, Kirtland Air Force Base, Albuquerque, NM. The authors wish to thank Dr. R. S. Erwin for his technical assistance.

References

[1] P. Y. Bely, Ed., *The Design and Construction of Large Optical Telescopes*, Springer, New York, 2003.

[2] P. D. Olivier, "Neuro-Fuzzy Phasing of the SIBOA Segmented Mirror Testbed," *Wavefront Sensing and Control Conference*, Kona, Hawaii, November, 2000.

[3] G. W. Zeiders, "Diffraction Effects with Segmented Apertures," in *Astronomical Telescopes and Instrumentation, Proc. SPIE*, Vol. 3356, pp. 799–809, 1998.

[4] G. W. Zeiders, "Image-Based Alignment of Large Segmented Telescopes," in *Optical Design, Materials, Fabrication, and Maintenance, Proc. SPIE*, Vol. 4003, pp. 241–249, 2000.

[5] P. D. Olivier, "Global Nonlinear Observers," *Proc. IEEE Southeastern Symp. System Theory*, March, 2004.

[6] K. N. Schrader, R. H. Fetner, S. F. Griffin, and R. S. Erwin, "Development of a Sparse-Aperture Testbed for Optomechanical Control of Space-Deployable Structures," *Highly Innovative Space Telescope Concepts, Proc. SPIE* , Vol. 4849, Waikoloa, HI, December 2002.

[7] E. Hecht, *Optics*, 4th Edition, Addison Wesley Longman, Reading, 2002.

[8] N. N. Lebedev, *Special Functions and Their Applications*, Prentice Hall, Englewood Cliffs, NJ, 1965.